ISSN 1822-427X/eISSN 1822-4288
2022 Volume 17 Issue 4: 95–119
https://doi.org/10.7250/bjrbe.2022-17.581

THE BALTIC JOURNAL
OF ROAD
AND BRIDGE
ENGINEERING
2022/17(4)

NUMERICAL STUDY OF ROAD EMBANKMENT TYPE ACTION ON SHEAR STRESS AROUND SKEWED BRIDGE ABUTMENT

MAHDI ASADI[1], FOUAD KILANEHEI[1], AMIR MAHJOOB[2*]

[1]*Department of Civil Engineering,*
Imam Khomeini International University, Qazvin, Iran

[2]*Transportation Research Institute,*
Road, Housing and Urban Development Research Center, Tehran, Iran

Received 22 July 2021; accepted 28 April 2022

Abstract. This paper investigates the effect of different geometries of approach embankments and guides banks on the flow pattern and bed shear stress values in the skewed bridges in the compound channel using three-dimensional numerical modelling. First, the numerical model was evaluated based on the results of existing laboratory studies. After ensuring its proper performance, the elliptical guide bank and the three types of abutments: vertical-wall, spill-through, and wing-wall, at different skew angles are examined. Investigation of the values of maximum velocity and bed shear stress at the flow-conducting embankment and the flow-splitting embankment showed that in the flow-conducting embankment, the best performance is assigned to the elliptical guide bank. In contrast, the performance of various abutments is different for the flow-splitting embankment depending on the skew angle of the bridge. Then, different patterns based on streamlines for the geometry plan of the guide bank were proposed and studied. The results show that the most suitable pattern for the guide bank reduces the maximum flow velocity by up to 15% and

* Corresponding author. E-mail: a.mahjoob@bhrc.ac.ir

Mahdi ASADI (ORCID ID 0000-0002-2481-520X)
Fouad KILANEHEI (ORCID ID 0000-0001-8618-520X)
Amir MAHJOOB (ORCID ID 0000-0002-8973-5016)

reduces the maximum bed shear stress by up to 80% around the flow-splitting embankments.

Keywords: approach embankment, compound channel, FLOW-3D, flow pattern, guide bank, shear stress.

Introduction

Natural rivers usually consist of the main channel, which carries the base flow and a floodplain on one or both sides. The floodplain carries overbank flow during flooding, so the river acts as a compound channel. The hydraulic conditions of the flow in compound channels are different from simple ones. Due to the section's shape change and significant difference in the roughness of the main channel and floodplains, the flow structure in the compound channel is more complicated than in the simple channel.

Besides, bridges built over the rivers are among the most important river structures. Every year, many bridges worldwide are destroyed, not because of structural issues but due to the lack of consideration of the hydraulic factors in their design (Wardhana & Hadipriono, 2003). The river bed erosion at the bridge site is the most critical hydraulic factor of

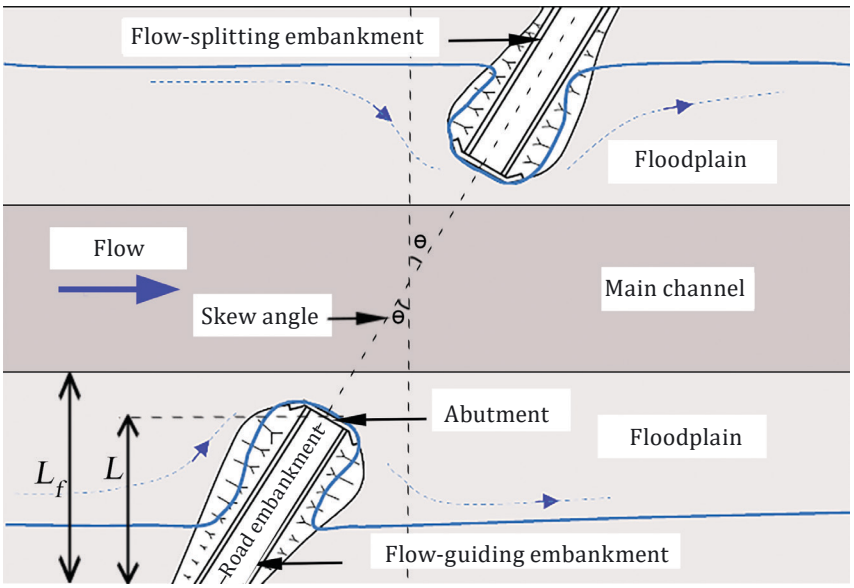

Figure 1. Illustration of the plan of a skewed bridge with θ angle in a compound channel

bridge destruction. Changes in the amount and direction of flow velocity at the bridge site cause increasing shear stress on the riverbed and move the bed particles that cause erosion.

Also, at the bridge section, usually to reduce the length of the bridge deck for economic issues, a part of the river floodplain is blocked by the road embankment. The embankments that are located in river floodplains reduce the flow cross-section. Figure 1 shows the plan of a skewed bridge with θ angle in a compound channel (Zevenbergen et al., 2012). In this paper, the ratio of the length of the embankment (L) to the floodplain length (L_f) is called the encroachment ratio (L/L_f).

According to their locations in the flow path and encroachment ratio, embankments of the skewed bridge may complicate the hydraulic flow conditions compared to the common crossing (skew angle = 0°) at the bridge site. Skewed bridge may increase the risk of erosion around the abutments.

Various researchers have considered study on these issues. Al-Khatib & Dmadi (1996) investigated the boundary shear stress distribution in a compound channel comprising a rectangular main channel and two symmetrically floodplains. Some significant results concerning the shear stress distribution are significant in alluvial channels to state the possible locations of erosion and deposition. Kouchakzadeh & Townsend (1997) found in their experiments that shear stress and scour depth increase in front of the abutment with increasing the encroachment ratio. Shiono & Knight (1988), by developing a quasi-two-dimensional model based on the Navier-Stokes equations, found the first step for applied mathematical modelling of hydraulic flow in compound channels. Biglari & Sturm (1998) performed numerical modelling of flow around bridge abutments located on the floodplain of a compound channel. They developed a two-dimensional depth-averaged model and used the two equation k-ε turbulence model. The numerical model results for velocity and flow depth are compared with laboratory data. They found a reasonable agreement between the numerical results and experimental data.

Molinas et al. (1998) conducted the experiments on vertical-wall abutments in a simple channel for Froude numbers ranging from 0.30 to 0.90 and for encroachment ratios of 0.1, 0.2, and 0.3. Shear stresses around the vertical-wall abutments are increased up to 10 and 1.5 times upstream shear stresses and velocities. Seckin (2007) performed some experiments concerning backwater at bridge constrictions placed in a compound channel flume with both common and skewed bridges. A new design chart is proposed for estimating backwater. Erduran et al. (2012) investigated the performance of FLOW-3D in predicting the water surface profiles at the location of the skewed bridges in the compound

channel. The experiments were carried out for four types of bridge models with two different skew angles (= 30° and = 45°). The comparison of free-surface profiles of the 3D model showed good agreement with the experimental data.

Fernandes et al. (2012) investigated the flow structure in a compound channel. They analysed the effect of floodplain roughness on the flow velocity and Reynolds stresses. They found that the velocity gradient and the Reynolds stresses increase with roughness. Morales & Ettema (2013) investigated the effect of embankment length on the flow velocity and bed shear stress in an asymmetric compound channel using laboratory and two-dimensional numerical models. They considered the encroachment ratios of 0.3, 0.5, 0.7, and 0.9. The results showed that increases in velocity were more noticeable near the front of the abutment. The maximum shear stress occurs upstream of the abutment, and as the length of the embankment increases, so does the amount of shear stress. Shahhosseini & Yu (2019) investigated four piers with different shapes. The results showed that the scouring depth depended on the shape of the bridge pier and the skew of its location in the flow. The best form of the piers, the smallest scouring around it, was the rhombus 30°, rhombus 60°, oblong and cylindrical, respectively. In another experiment, Yang et al. (2019) studied typical piers in both common and skewed piers to the flow. They found that the skewed piers increased the scouring rate around the piers significantly.

Chua et al. (2019) investigated the effect of encroachment ratio on the flow structure in an asymmetric compound channel with two floodplains. The results showed that the encroachment ratio significantly affected the flow velocity and the type of formation of vortices around the embankments. Ahmed et al. (2020) investigated the complex 3D flow structures with the vertically layered vegetation placed over the floodplains in a compound channel using FLUENT software. The results showed that the flow velocities were significantly reduced in the floodplains, resulting in an increased percentage of passing discharge through the main channel. Mahjoob & Kilanehei (2020) investigated the effects of the skewed bridge angle and encroachment ratio on the velocity and bed shear stress in a compound channel using a developed 3D numerical model. The results showed that the bed shear stress around the flow-conducting embankments decreases with increasing the skew angle. But there has been an increasing trend around flow-splitting embankments. The trend of the maximum shear stress variations around the flow-splitting abutment was different for different encroachment ratios; at an encroachment ratio of 0.25, it was the highest at a 45°, but for encroachment ratios of 0.50 and 0.75, it was the maximum at a 30° and reduced at a 45°.

Some numerical and experimental studies have been performed on the flow pattern, bed shear stress, and scouring around the access embankments of bridges in compound channels. However, a simultaneous study of the performance of different access embankment forms in skewed bridges with different angles has received less attention. In this study, three-dimensional numerical simulations of the flow using FLOW-3D software around four types of abutments with five different skew angles (0°, 10°, 20°, 30°, and 40°) are performed, and the values of maximum velocity, and bed shear stress around the flow-conducting and flow-splitting embankments were analysed. Also, a new proposed pattern based on streamlines is presented for the guide bank, in order to improve the hydraulic conditions of the flow through the bridge.

1. Materials and methods

1.1. Basic embankment shapes and elliptical guide bank

Figure 2 illustrates the elliptical guide bank and the three common abutment shapes: vertical-wall, spill-through, and wing-wall, which have been examined in this paper.

Most references recommend using guide banks with a planform shape of a quarter of an ellipse, with the ratio of the major axis to the minor axis of 2.5:1 (Mays, 2010).

The width and height of all embankments were respectively selected at 11 m and 7 m based on the width of the road and the maximum water

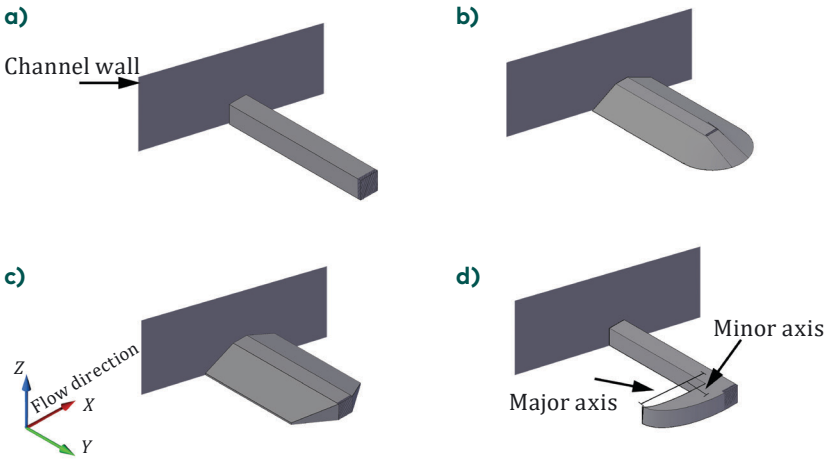

Figure 2. 3D views of basic embankment shapes: a) vertical-wall; b) spill-through; c) wing-wall; d) elliptical guide bank

level at the bridge site. The embankment side slope for the spill-through and the wing-wall were considered with a ratio of 2:1 (horizontal to vertical).

1.2. Numerical modelling

The commercially available CFD program, FLOW-3D, is now prevalent and is used in research and industry. This software was selected for this study.

FLOW-3D model can simulate water flow, sediment transport and scour and is suitable for three-dimensional hydraulic simulations.

The model simultaneously solves the three-dimensional Navier-Stokes equations and the continuity equation. The continuity (Equation (1)) and the Navier-Stokes equations for incompressible flows (Equations (2)–(4)) are as follows (Smith & Foster, 2005):

$$\frac{\partial}{\partial x_i} u_i A_i = 0, \tag{1}$$

$$\frac{\partial u_i}{\partial t} + \frac{1}{V_\mathrm{f}}\left(u_j A_j \frac{\partial u_i}{\partial x_j} \right) = -\frac{1}{\rho}\frac{\partial P}{\partial x_i} + G_i + f_i, \tag{2}$$

where

$$\rho V_\mathrm{f} f_i = \tau_{b,i} - \left[\frac{\partial}{\partial x_j}\left(A_j S_{ij} \right) \right], \tag{3}$$

$$S_{ij} = -\mu_\mathrm{total}\left[\frac{\partial u_i}{\partial x_j} + \frac{\partial u_j}{\partial x_i} \right], \tag{4}$$

where u_i – mean velocity, m/s; P – pressure, kg m^{-1} s^{-2}; A_i – fractional area on to flow in the i direction; V_f – fractional volume open to flow; G_i represents the body accelerations, m/s^2; f_i represents the viscous accelerations, m/s^2; S_{ij} – strain rate tensor, kg m^{-1} s^{-2}; $\tau_{\mathrm{b},i}$ – wall shear stress, kg m^{-1} s^{-2}; ρ – density of water, kg/m^3; μ_total – total dynamic viscosity, which includes the effects of turbulence ($\mu_\mathrm{total} = \mu + \mu_\mathrm{T}$), kg m^{-1} s^{-1}; μ – dynamic viscosity, kg m^{-1} s^{-1}; μ_T – eddy viscosity, kg m^{-1} s^{-1}.

The model has available several different turbulence closure schemes, including one-equation turbulent energy (k), two-equation (k-ε), renormalisation-group (RNG), and large eddy simulation (LES) closure schemes.

The wall boundary conditions are evaluated differently based on the chosen turbulence closure scheme. Transport turbulence closure schemes, e.g., the k-ε model, use a law of the wall formulation. The combined smooth and rough logarithmic law of the wall Equation (5) is iterated to solve for the shear velocity (Flow Science, Inc., 2002):

$$u_o = u_* \left[\frac{1}{k} \ln \left(\frac{\rho u_* y_o}{\mu + \rho a u_* k_s} \right) + 5.0 \right], \quad (5)$$

where u_* is the shear velocity, m/s; k – von Karman constant; a is a constant, which is equal to 0.247 for k-ε and RNG models, or 0.246 otherwise; k_s is the roughness, m; and y_o – distance, from the solid wall to the location of tangential, m; u_o – velocity, m/s.

The denominator of Equation (5) represents an effective viscosity because of the rough boundary:

$$\mu_{eff} = \mu + \rho a u_* k_s. \quad (6)$$

Wall shear stress, $\tau_{b,i}$, is defined with Equation (7):

$$\tau_{b,i} = \rho(u)^2. \quad (7)$$

1.3. Verification

The laboratory data of Morales & Ettema (2013) and Seckin (2007) have been used, in order to ensure the proper performance of the numerical model.

1.3.1. Morales & Ettema laboratory model

Morales & Ettema (2013) investigated the effect of embankment length on the flow velocity and bed shear stress in an asymmetric compound channel. Figure 3 shows the plan and cross-section of the laboratory channel.

The length of the spill-through abutment (L) is considered in two cases: 1.22 m and 2.44 m. The abutments are placed at a distance of

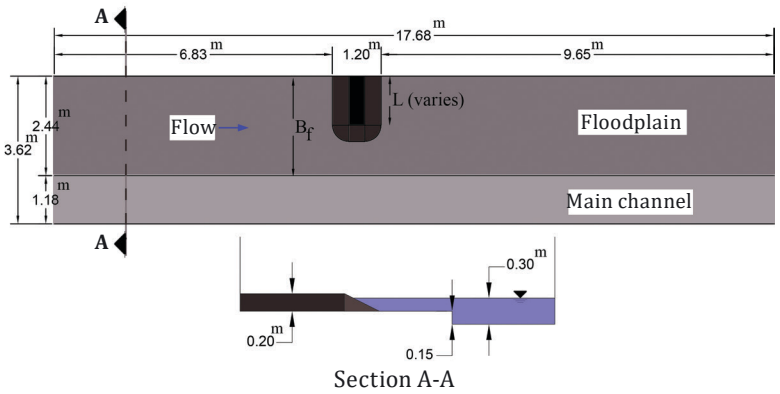

Figure 3. Plan and cross-section of Morales & Ettema's (2013) laboratory channel

7.43 m from the upstream, and the total length of the channel is 17.68 m. The floodplain bed was elevated 0.15 m above the flume bottom that formed the main channel bed, and the flow rate was 0.3 m^3/s. The model was simulated in FLOW-3D software. Upstream and downstream boundary conditions have been considered volume flow rate and specified pressure, respectively. For the walls and floor of the channel, the wall boundary condition has been set, and for the free surface of the water, the symmetry boundary condition has been set.

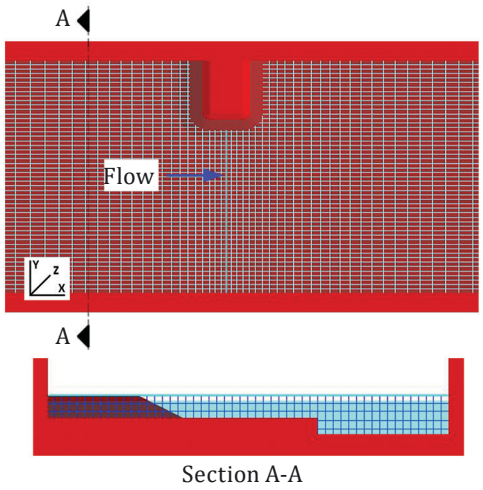

Figure 4. Computational grid: 2D mesh and cross-section for Morales & Ettema (2013) laboratory model

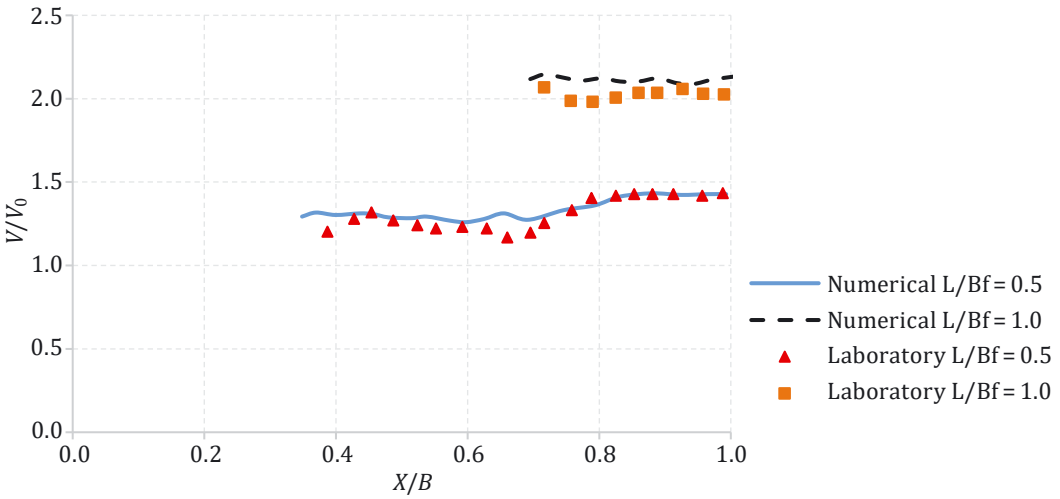

Figure 5. Comparison of model results and experimental measurements at cross-section passing through abutment centerline

The model was made in FLOW-3D software based on the above. Figure 4 shows the computational grid and the mesh block of the model. The mesh sizes increased away from the abutment (further upstream and downstream of the structures) to decrease the computation cost. The height of meshes in the Z direction is considered to be 0.07 m.

Figure 5 compares numerical model results with laboratory measurements, where V is the depth-averaged velocity, V_0 is the depth-averaged velocity in the approach flow, X is the distance measured along the cross-section, and B is channel half-width.

To evaluate the results obtained from the numerical model, the error values of calculating the longitudinal averaged velocities numerically with laboratory model results have been determined using the root-mean-square error (Equation (8)).

$$RMSE = 100\sqrt{\frac{1}{N}\sum_{i=1}^{N}\left(V_i^{\exp} - V_i^{\text{num}}\right)^2}. \tag{8}$$

where $V_i^{\exp}$ is laboratory values (m/s), V_i^{num} is metric values (m/s), and N is the number of data values. The RMSE values in different cases of abutment length of 1.22 m and 2.44 m were about 4.3% and 7.1%, respectively, an acceptable range of error values between numerical and laboratory modelling.

1.3.2. Seckin laboratory model

Seckin (2007) performed some experiments concerning backwater at bridge constrictions placed in a compound channel flume with both regular and skewed bridges. A new design chart is proposed for estimating backwater. Figure 6 shows the laboratory plan view of the Seckin laboratory model.

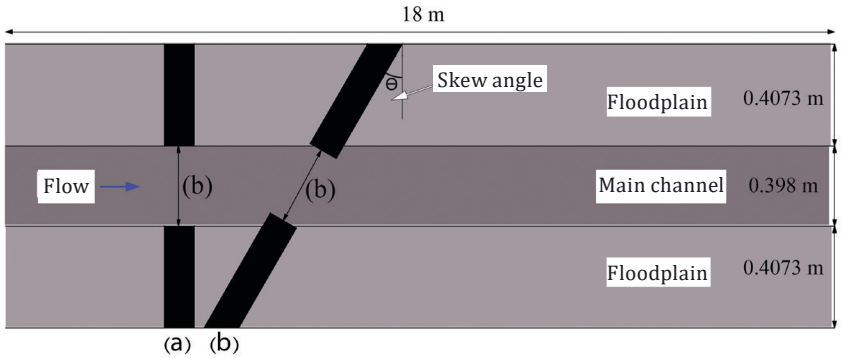

Note: (a) – common crossing and (b) – skewed bridge (skew angle = 30°).

Figure 6. Plan view of Seckin's (2007) laboratory channel

The length of the channel is 18 m. The width of the main channel and the two floodplains are 0.398 and 0.4073 m, respectively. The channel slope was 0.002024, and the flow rate was 0.021 m^3/s.

It should be noted that the bridge opening width (b = 0.3980 m) was not changed in the experiments and numerical modelling for the skewed bridges. The flow rate was 0.0567 m^3/s. According to the laboratory model, the numerical model was simulated in FLOW-3D software.

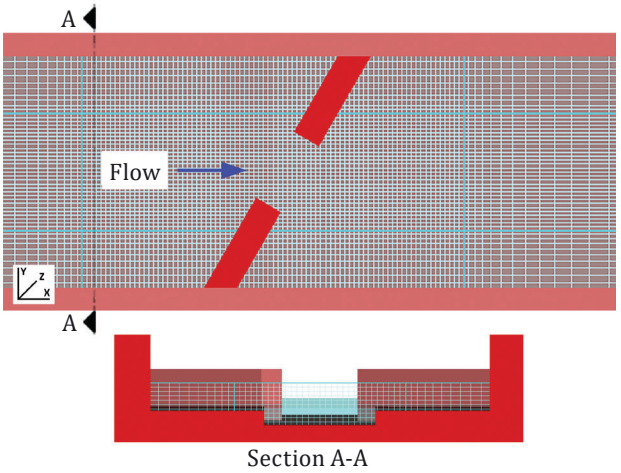

Figure 7. Computational grid: 2D mesh and cross-section for Seckin's (2007) laboratory model at a 30° skew angle

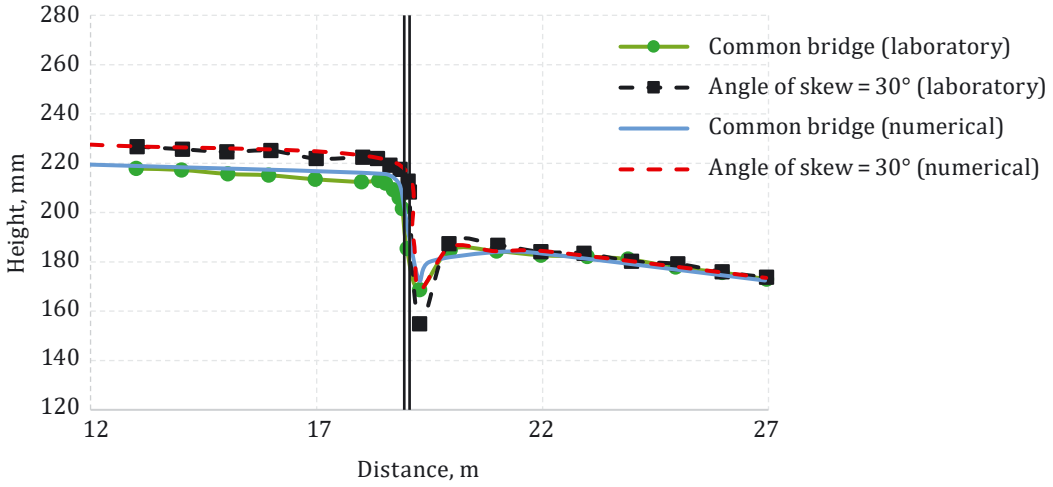

Figure 8. Water level profiles obtained from the results of the numerical models and the results of Seckin laboratory models

Table 1. Values of RMSE for water level profiles numerically and Seckin (2007) laboratory models

Skew angle	Numerical model error rate, %		
	area 1	area 2	area 3
0°	1.0	2.6	0.5
30°	1.5	13.4	0.5

Figure 7 shows the geometric field and computational grid performed for numerical modelling of the 30° skew angle. Around the abutment, and especially on the abutment's nose, a finer mesh is provided to achieve higher accuracy. The height of meshes in the *Z* direction is considered to be 0.015 m.

Figure 8 shows the water level profiles obtained from the numerical and laboratory model results.

The error rate of calculating water level profiles by the numerical models with laboratory models using the RMSE is presented in Table 1, in order to evaluate the results obtained from the numerical model. For this purpose, as seen in Figure 8, the channel length has been divided into three areas for a more detailed analysis. The error range between numerical and laboratory modellings in areas 1 and 3 is negligible for both models and area 2 only for the common crossing. Although at the skew of 30°, the error value in area two is high but acceptable. It can be considered due to the error of the numerical model because of the significant turbulence in this area.

1.4. Geometric and hydraulic specifications of the model

This paper studied flow patterns around the abutments and the embankments of skewed bridges in the floodplain of compound channels. The symmetrical trapezoidal compound channel is used, and the cross-section of the channel is shown in Figure 9. The sidewall of the trapezoidal section has a skew of 45° in the main channel and the floodplains. The width of the floodplain and the main channel is 140 m

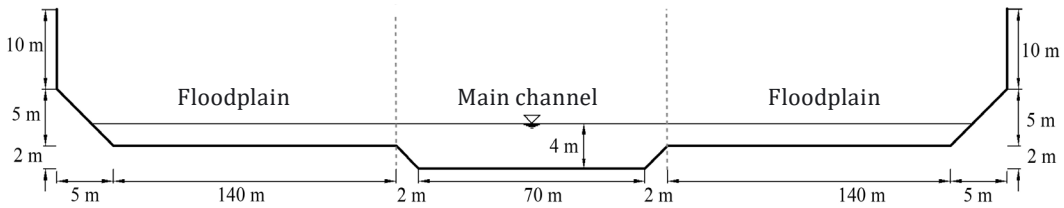

Figure 9. Cross-section view of the compound channel

and 70 m, respectively. The channel length is 3000 m, the slope of the channel bed is 0.002, and the roughness coefficient of the floodplain and the main channel are 0.05 and 0.03, respectively.

The channel inlet flow rate is 1865 m^3/s. Determining the dimensions of the desired compound channel is based on the authors' experience. In natural rivers, the floodplain's width is mainly greater than the main channel, which is considered in cross-sectional dimensions. For more compatibility with nature, the slope of the channel walls and the floodplain's junction to the main channel is 45°.

1.5. Determining the appropriate encroachment ratio

First, the simple compound channel model is simulated as a basic model to make the test results dimensionless. To perform tests related to the effect of the skewed bridge, other parameters, including the encroachment ratio, needed to be constant. Various simulations have been performed on the vertical-wall abutment with 40%, 50%, 60%,

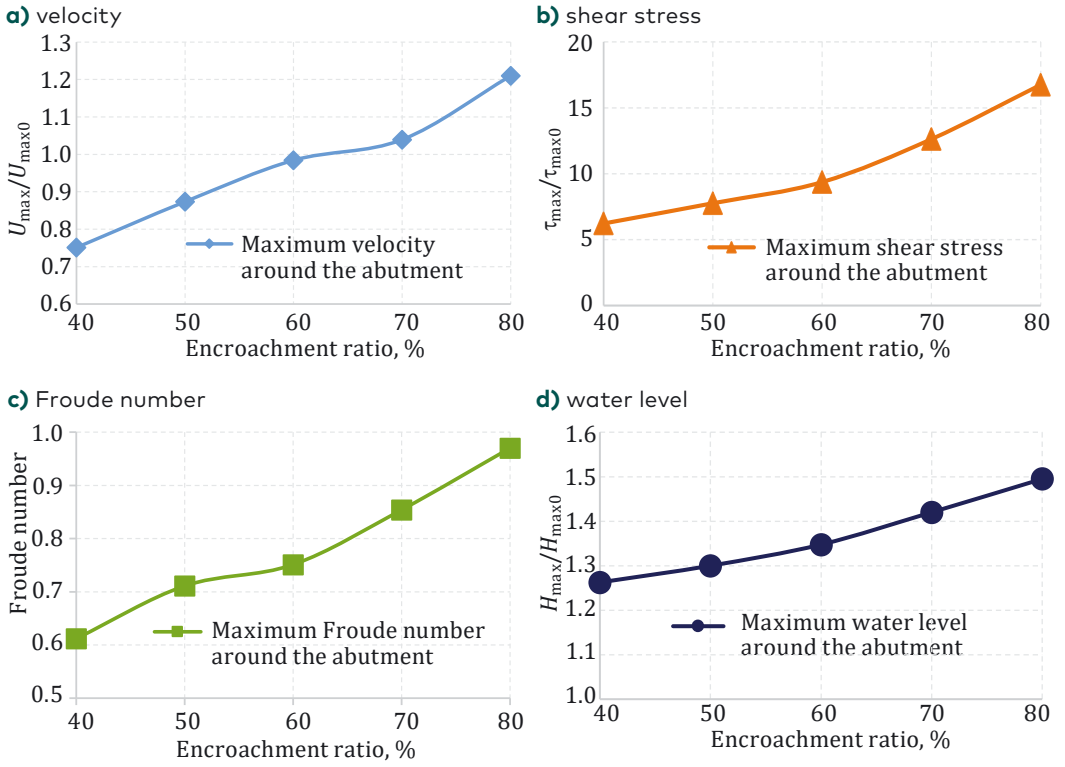

Figure 10. Results of tests related to determining the constant encroachment

70%, and 80% encroachment ratios for use in skewed bridge tests. Figure 10 shows the dimensionless results for velocity, bed shear stress, Froude number, and the water level around the abutment.

In Figure 10, subscript "max" is related to the hydraulic parameters around the abutment, and subscript "max_0" is related to the hydraulic parameters in the base model. U, τ and H are the flow velocity, the bed shear stress and the water level, respectively.

With the increase of the encroachment ratio from 40% to 80% (Figure 10), velocity, bed shear stress, Froude number, and water level increased by 38%, 63%, 37%, and 23%, respectively.

As can be seen from the results, the parameters of velocity, bed shear stress, Froude number, and water level increase the risk of scouring, and water entering the lands around floodplains increases sharply after 50% of the encroachment ratio. Therefore, the constant encroachment ratio for skewed bridge tests, 50%, equivalent to 72.5 m, has been selected.

2. Results and discussion

The simulations were performed in four different cases of the embankment (Figure 2) and five skew angles (0°, 10°, 20°, 30°, and 40°) with a 50% encroachment ratio.

After different studies, three nested meshes are considered in each test. The first grid is related to the whole computational domain, the length of which is equal to the total length of the channel (3000 m), and its width is equal to the total width of the channel (364 m). The second grid starts in the longitudinal direction from 100 m upstream of the flow-guiding embankment and continues up to 150 m downstream of the flow-splitting embankment, and its width follows the width of the first grid. The third grid is considered in proportion to the skew angle and embankment type in the area around the embankments. The dimensions of the third grid are smaller than the dimensions of the second grid, and the dimensions of the second grid are smaller than the dimensions of the first grid. The height of meshes in the Z direction for the mesh blocks, from the largest to smallest, were considered 1.5 m, 0.8 m, and 0.5 m, respectively.

FLOW-3D solves the fully three-dimensional transient Navier-Stokes equations using the Fractional Area/Volume Obstacle Representation (FAVOR) and the volume of fraction method. The first-order momentum advection formulation was used as the discretisation method. The implicit solver, GMRES[1], was used in the numerical simulation. The

1 Generalized Minimal Residual method

solver uses finite volume approximation to discretise the computational domain. FLOW-3D uses the VOF method to track the free surface.

Figure 11 shows a cross-section and plan mesh grid of flow-splitting embankments for a 30° skew (for example) for different cases.

Before performing the simulation, some settings have been done for the model. The k-ε method has been used to simulate turbulence. The volume flow rate with the corresponding water level is applied as a boundary condition at the entrance border of the domain (upstream). The outlet domain (downstream) selects the specified pressure boundary condition. The sidewalls, as well as the channel bottom, were set as a wall. Finally, on the top, the boundary was set as symmetry to account for the atmospheric pressure on the free surface.

The models are simulated. Then, the maximum values of velocity and bed shear stress around the flow-guiding and flow-splitting embankments are extracted from the results. In Figures 12 and 13, to provide the flow pattern, the velocity distribution plan at the height of 1 m from the floodplain bed is presented for flow-guiding and flow-splitting embankments at a skew of 30° (for example) for different cases, respectively.

Figures 14 and 15 show the dimensionless diagrams of the maximum velocity and bed shear stress around the flow-guiding and flow-splitting embankments for the four mentioned cases at different skew angles (0°, 10°, 20°, 30°, and 40°), respectively.

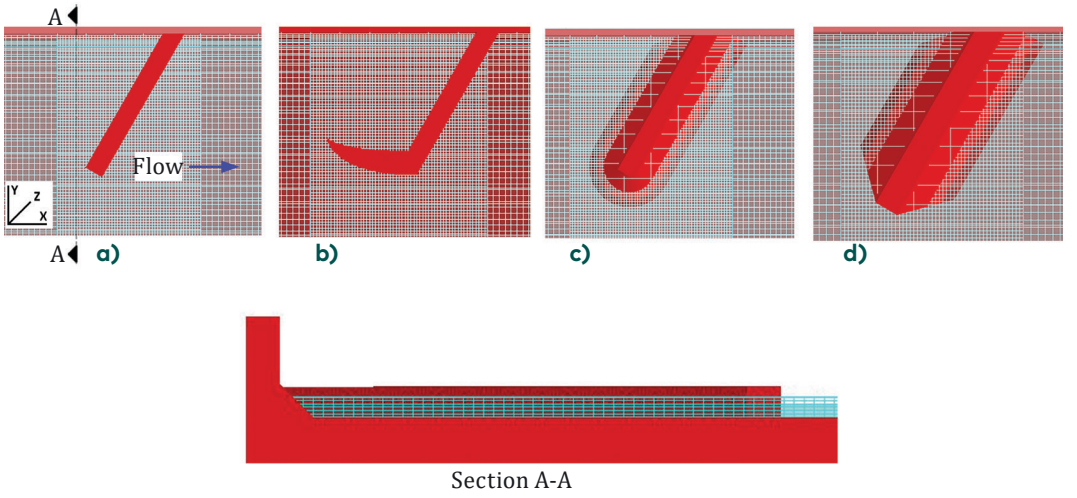

Figure 11. Cross-section and plan mesh grid for the flow-splitting embankment for a 30° skew: a) vertical-wall; b) elliptical guide bank; c) spill-through; d) wing-wall

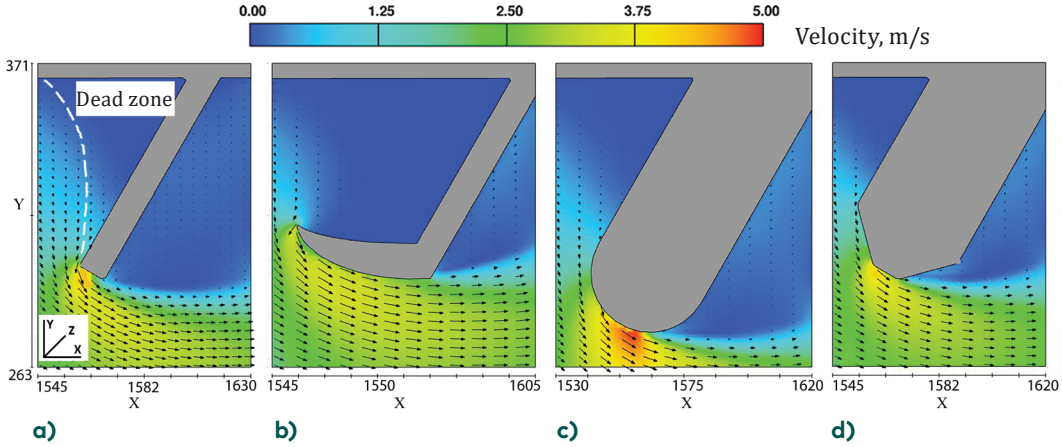

Figure 12. Velocity distribution at the height of 1 m from the floodplain bed for flow-splitting embankment at a 30° skew angle: a) vertical-wall; b) elliptical guide bank; c) spill-through; d) wing-wall

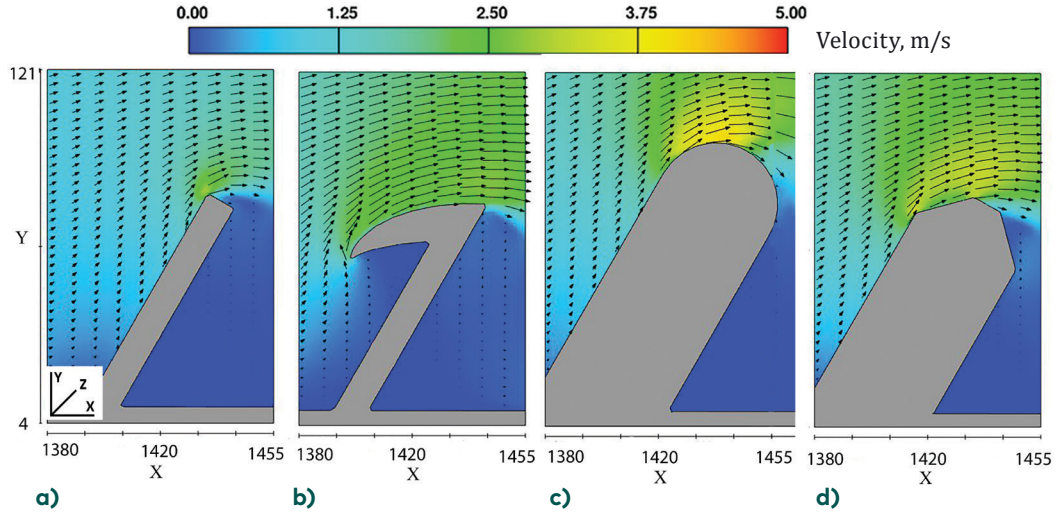

Figure 13. Velocity distribution at the height of 1 m from the floodplain bed for flow-guiding embankment at a 30° skew angle: a) vertical-wall; b) elliptical guide bank; c) spill-through; d) wing-wall

Figures 14a and 14b show that with increasing bridge skew angle from 0° to 40°, the maximum velocity and shear stress around the flow-guiding embankment for all four cases decrease. It can be concluded that the embankment acts as a guide bank and will improve the flow transfer to the bridge span by increasing the skew angle. Among the flow-guiding embankments, the elliptical guide bank performs better than other abutments due to the lower rate of velocity and bed shear stress around the abutment at different skew angles.

In Figures 15a and 15b, with the increasing skew angle from 0° to 10°, the maximum velocity and bed shear stress around the flow-splitting embankments for all four cases increase. Increasing the skew angle

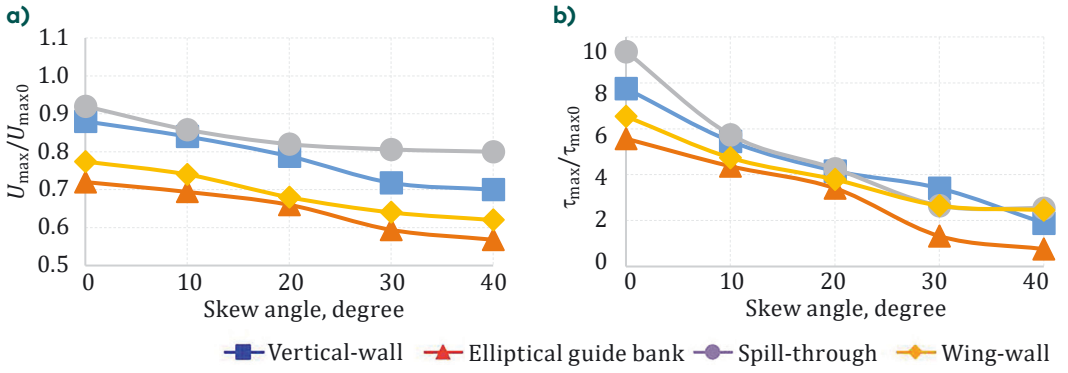

Figure 14. Diagram of velocity and shear stress changes for different cases: a) maximum velocity diagram around the flow-guiding embankment; b) maximum shear stress diagram around the flow-guiding embankment

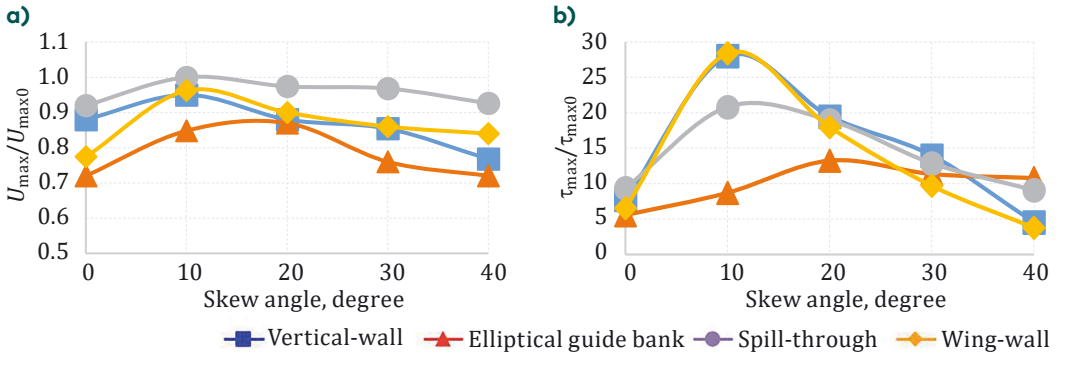

Figure 15. Diagram of velocity and shear stress changes for different cases: a) maximum velocity diagram around the flow-splitting embankment; b) maximum shear stress diagram around the flow-splitting embankment

from 10° to 40° increases the maximum velocity and bed shear stress for all cases except the elliptical guide bank decrease. This unexpected situation of the elliptical guide bank may be attributed to forming of a dead rotational zone upstream of the flow-splitting embankments, which can ease the passage of water like a guide bank (Figure 12a). Among flow-splitting embankments, the elliptical guide bank at lower skew angles (0° to 20°) and wing-wall for higher skew angles (30° to 40°) have lower bed shear stresses than other abutments. The weak performance of the elliptical guide bank at high skew angles can be considered due to its geometric shape and placement position in the water flow.

Table 2 examines the quantitative values of the results extracted from the diagrams in Figures 14 and 15. In the columns related to the flow-guiding and flow-splitting embankments, the rate of change of both, velocity ratio and bed shear stress ratio for all cases and skew angles (as a percentage) is presented. In this Table 2, the sign (+) indicates an increase, and the sign (–) indicates a decrease in the amount of these changes within the specified range.

In Table 2, in the case of increasing bed shear stress, wing-wall, vertical-wall, and spill-through with +76%, +73%, and +54%, respectively, have the highest increase ratio in bed shear stress in the specified range. On the other hand, in the case of reducing bed shear stress ratio, vertical-wall, elliptical guide bank, and wing-wall with −68%, −62%, and −61%, respectively, have the highest amount of bed shear stress reduction in the specified range.

Table 2. Rate of change of velocity ratio and bed shear stress ratio in different cases

Case	Parameter, %	Flow-guiding embankment, skew angles, °				Flow-splitting embankment, skew angles, °			
		0–10	10–20	20–30	30–40	0–10	10–20	20–30	30–40
Vertical-wall	Velocity	–5	–7	–9	–13	+8	–8	–3	–11
	Shear stress	–30	–24	–19	–45	+73**	–31	–29	–68*
Elliptical guide bank	Velocity	–4	–5	–10	–5	+16	+3	–13	–6
	Shear stress	–28	–28	–62*	–43	+37	+35	–15	–5
Spill-through	Velocity	–7	–5	–2	–1	+8	–3	–1	–5
	Shear stress	–29	–26	–38	–5	+54**	–10	–32	–30
Wing-wall	Velocity	–5	–9	–6	–4	+20	–7	–5	–3
	Shear stress	–28	–20	–30	–8	+76**	–37	–47	–61*

Note: * – the highest increase ratio; ** – the highest decrease ratio.

Figure 16 shows the diagram of the ratio of bed shear stress reduction to velocity reduction in the flow-guiding embankment for all cases and skew angles. In this Figure 16, the rate of change of the mentioned parameters has been considered between the highest and lowest values (decreasing or increasing trend) among all skew angles. For example, the ratios of change in maximum velocity and bed shear stress in the spill-through case between the two skew angles of 0° to 40° is -14% and –73%, respectively, and the number 5.2 shown in the diagram in Figure 16 is the result of dividing the number 73 by 14. As the velocity decreases, the bed shear stress decreases by about 5.2 times the velocity reduction.

The results show, in the flow-guiding embankment, the performance of the elliptical guide bank is better than in the other cases. In this case, the numerical value of maximum velocity and maximum bed shear stress is less than in the other cases. Besides, the ratio of bed shear stress reduction to velocity reduction also occurs at a high rate (Figure 16). While in the flow-splitting embankment, the optimal case is unknown, and the elliptical guide bank performs better in lower skew angles. Its performance in higher skew angles is not approved. Although the numerical value of maximum velocity is lower than in the other cases, the ratio of bed shear stress reduction occurs at a much lower rate than in other cases. Therefore, to resolve this problem, the geometry of the guide bank for its better functioning in the skewed bridge, especially at the flow-splitting embankment, is investigated and presented in the next part.

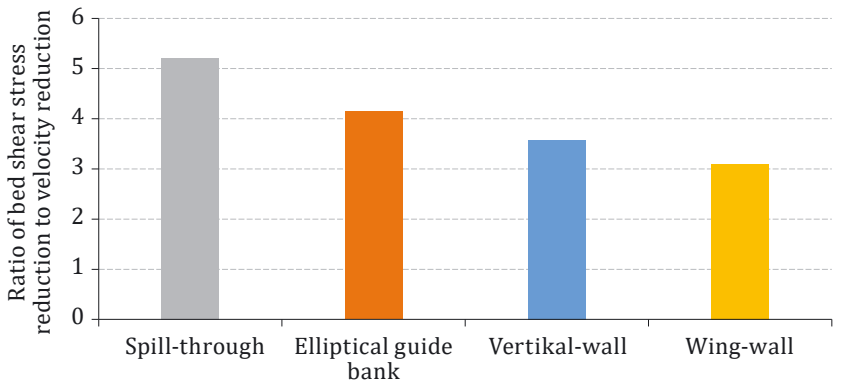

Figure 16. Diagrams of the ratio of bed shear stress reduction to velocity reduction in the flow-guiding embankment in different cases

3. New suggested geometries to improve performance of guide bank

Around the embankments, the flow passage will be accompanied by significant turbulence due to changes in direction and the magnitude of the flow velocity at the abutment's nose (especially around the flow-splitting abutment). The purpose of constructing the guide bank is to gently pass the flow through the bridge span so that the flow is accompanied by minimal turbulence. If the guide bank is constructed so that its geometric shape does not conflict with the streamline passing through the bridge span, there will be no confrontation between the guide bank and the streamline, and as a result, the guide bank will perform better. Thus, the proposed patterns for better guide bank performance are inspired by the streamlines from the bridge span.

The proposed patterns are presented and examined in three patterns according to the streamlines formed in vertical-wall simulations. According to Figure 17, the proposed design of pattern No. 1 is according to the streamlines passing through the nose of the abutment. The proposed patterns of patterns No. 2 and No. 3 are according to

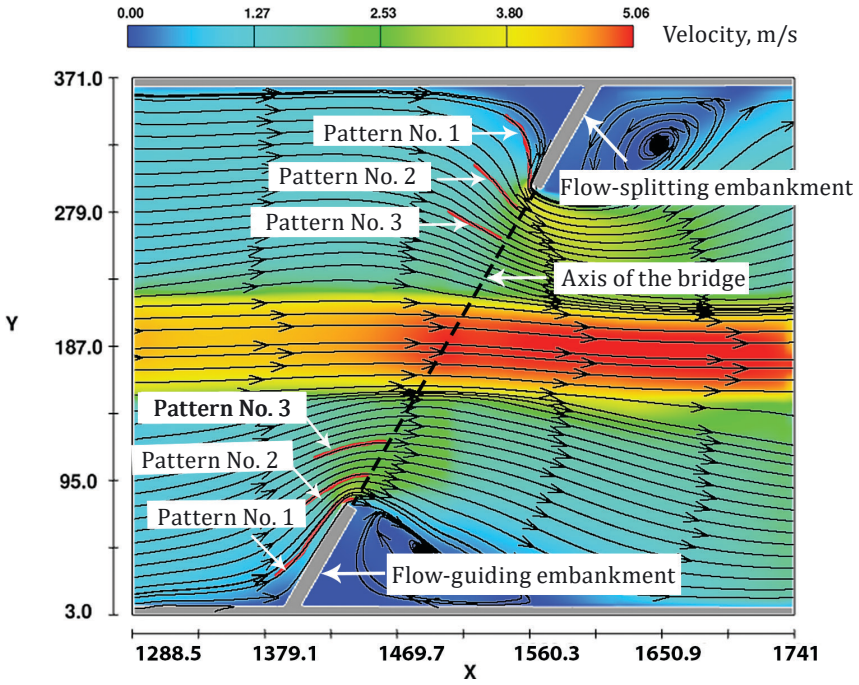

Figure 17. View of the plan for velocity distribution and streamlines formed around a vertical-wall at a skew of 30°

the streamlines passing through the distance of 25% and 50% of the abutment nose to the floodplain and main channel border, respectively (along the bridge's axis). These patterns are simulated for 0°, 10°, 20°, 30°, and 40° skew angles. The length of the guide bank is considered for the proposed patterns as in the previous part.

Figure 17 shows the streamlines for the proposed guide bank patterns for flow-guiding and flow-splitting embankments at a skew of 30° (for example) for different patterns.

Figure 18 shows the geometry plan of proposed patterns for the guide bank at a skew of 30°.

The flow simulation was performed for all three patterns, and then the maximum values of velocity and bed shear stress around the flow-guiding and flow-splitting embankments were extracted. Figures 19 and 20 show the velocity distribution plan for flow-splitting and flow-guiding embankments at a skew of 30° (for example) for different patterns, respectively.

Figures 21 and 22 show the dimensionless diagrams of the maximum velocity and maximum bed shear stress around the flow-guiding and flow-splitting embankments for the three patterns and also the elliptical guide bank at different skew angles (0°, 10°, 20°, 30°, and 40°), respectively.

In Figures 21a and 21b, with increasing the abutment skew angle from 0° to 40°, the maximum velocity and bed shear stress around the flow-guiding embankment for all three patterns, according to Table 3, decrease. Among the flow-guiding embankments, the elliptical guild bank and pattern No. 3 perform better in velocity reduction than the others.

Figures 22a and 22b present that increasing the skew angle from 0° to 10° increases the maximum velocity and bed shear stress around the flow-splitting embankments for all three proposed patterns. While increasing the skew angle from 10° to 40°, the maximum velocity and bed shear stress for all patterns have a decreasing trend. Among

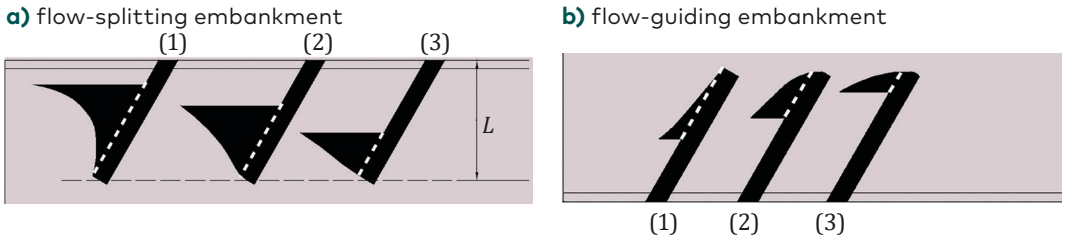

Figure 18. Geometry plan of proposed patterns for guide bank at a skew of 30°

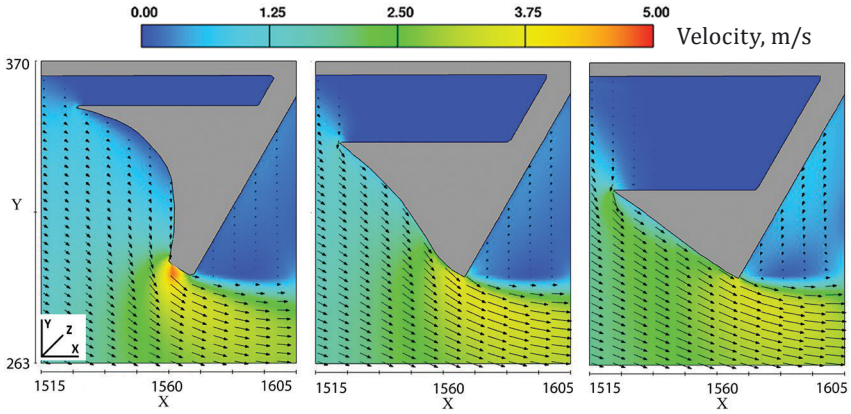

a) pattern No. 1 **b)** pattern No. 2 **c)** pattern No. 3

Figure 19. Velocity distribution at the height of 1 m from the floodplain bed for flow-splitting embankment at a 30° skew angle

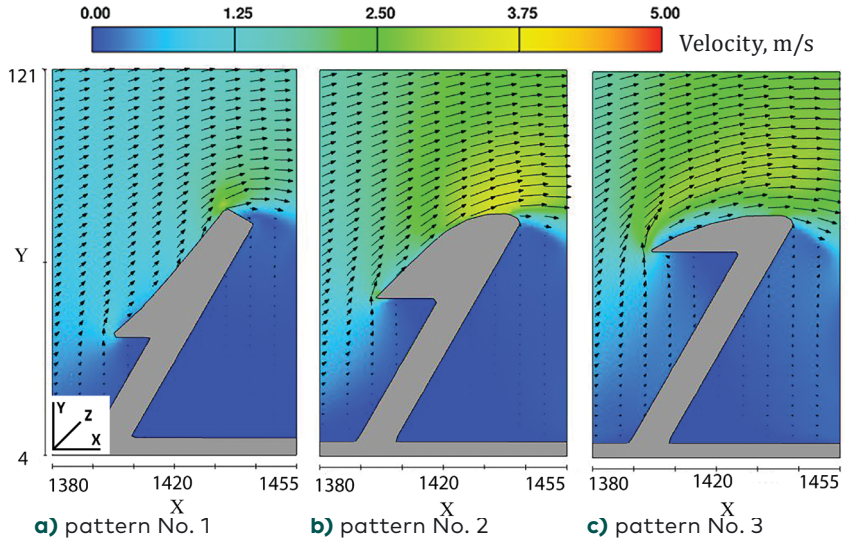

a) pattern No. 1 **b)** pattern No. 2 **c)** pattern No. 3

Figure 20. Velocity distribution at the height of 1 m from the floodplain bed for flow-guiding embankment at a 30° skew angle

flow-splitting embankments, the abutment with pattern No. 3 guide bank performs better than the other patterns.

According to the results reviewed in the tests related to the patterns and the elliptical guide bank, in the flow-guiding embankment, the performance of the elliptical guide bank is still better than the other patterns. Considering that, the results of this case are not much different from pattern No. 3 and have almost the same performance. While in the flow-splitting embankment, the proposed model of pattern

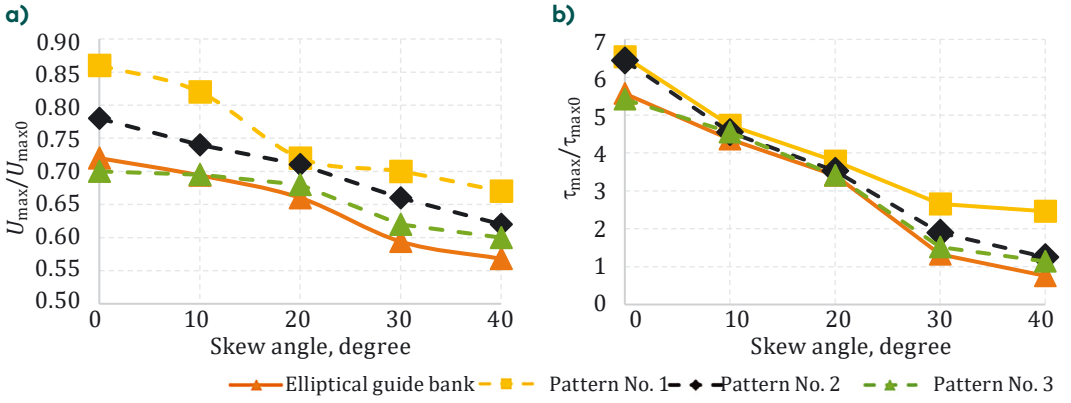

Figure 21. Diagram of velocity and bed shear stress changes for different patterns: a) maximum velocity diagram around the flow-guiding abutment; b) maximum shear stress diagram around the flow-guiding abutment

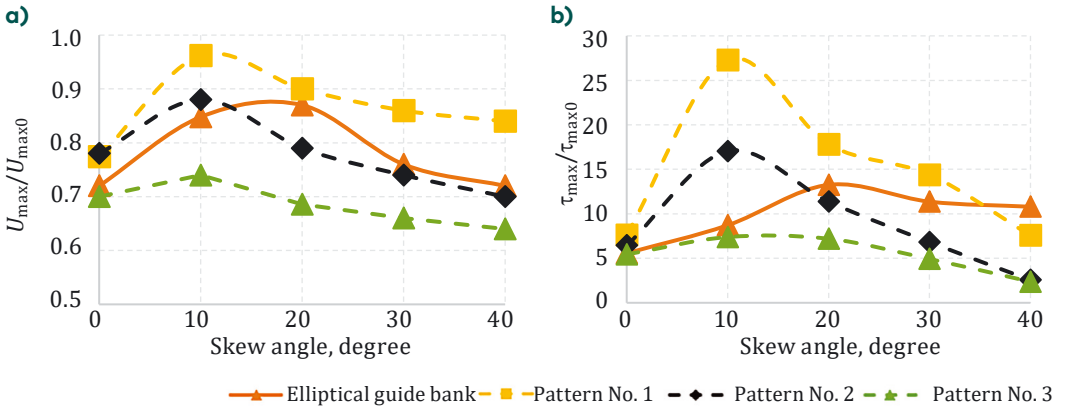

Figure 22. Diagram of velocity and bed shear stress changes for different patterns a) Maximum velocity diagram around the flow-splitting abutment: a) maximum velocity diagram around the flow-guiding abutment; b) maximum shear stress diagram around the flow-guiding abutment

No. 3 performs better than all patterns and cases. In this pattern, the numerical value of velocity and bed shear stress is less than in the other cases. The results show that the proposed pattern No. 3 for the guide bank reduces the maximum flow velocity by up to 15% and reduces the maximum bed shear stress by up to 80% around the flow-splitting embankments relative to the elliptical guide bank.

Conclusion

In this study, a three-dimensional simulation of the flow around the embankments of the skewed bridge in a compound channel has been considered to investigate the hydraulic parameters of the flow around the common types of embankment geometry and the elliptical guide bank. Since part of the floodplain is usually blocked by the embankment, the optimal encroachment ratio in the bridge was selected by analysing the different opening ratios. The flow simulation was performed for various common types and the elliptical guide bank at five different skew angles (0°, 10°, 20°, 30°, and 40°). The results showed that in the flow-guiding embankment, the shear stress decreases with increasing skew angle; it may even be inferred that the embankment acts as a guide bank and will improve the flow conditions transfer to the bridge span by increasing the skew angle. In the elliptical guide bank, the numerical value of velocity and bed shear stress is less than in the other cases. Furthermore, the bed shear stress reduction to velocity reduction is high. Unexpectedly, In the flow-splitting embankment, at skew angles above 10°, the hydraulic parameters decrease for all cases except the elliptical guide bank. This may be attributed to forming a dead rotational zone of the stream upstream of the flow-splitting embankments, which can ease the flow passage like a guide bank. In general, the performance of the elliptical guide bank is better in the flow-guiding embankment at all skew angles and in the flow-splitting embankment at the lower skew angles. The new patterns plan for the guide bank was proposed and studied according to the streamlines passing through the bridge span, in order to optimise the flow condition in crossing the bridge span, especially for the flow-splitting embankment. The results of these studies showed that the pattern corresponding to the streamlines passing from 50% of the distance from the nose of the abutment to the border of the floodplain and the main channel (along the axis of the bridge) reduces the maximum flow velocity by 15% and maximum bed shear stress up to 80% around the flow-splitting embankment relative to the elliptical guide bank. The model also performs better than other cases in the flow-splitting embankment. In this model, the numerical

value of velocity and bed shear stress is less than in the other cases. Besides, the ratio of bed shear stress reduction to velocity reduction also occurs at a high rate.

REFERENCES

Ahmad, M., Ghani, U., Anjum, N., Ahmed Pasha, G., Kaleem Ullah, M., & Ahmed, A. (2020). Investigating the flow hydrodynamics in a compound channel with layered vegetated floodplains. *Civil Engineering Journal, 6*(5), 860–876. https://doi.org/10.28991/cej-2020-03091513

Al-Khatib, I. A., & Dmadi, N. M. (1996). Boundary Shear Stress in Rectangular Compound Channels. *Journal of Engineering and Environmental Sciences, 23*(1), 9–18.

Biglari, B., & Sturm, T. W. (1998). Numerical Modeling of Flow around Bridge Abutments in Compound Channel. *Journal of Hydraulic Engineering, 124*(2), 156–164. https://doi.org/10.1061/(asce)0733-9429(1998)124:2(156)

Erduran, K. S., Seckin, G., Kocaman, S., & Atabay, S. (2012). 3D Numerical Modelling of Flow Around Skewed Bridge Crossing. *Engineering Applications of Computational Fluid Mechanics, 6*(3), 475–489. https://doi.org/10.1080/19942060.2012.11015436

Fernandes, J. N., Leal, J. B. and Cardoso, A. H. (2012). Flow structure in a compound channel with smooth and rough floodplains. *European Water, 38*(1), 3–12.

Flow Science, Inc. (2008). *FLOW-3D User's Manual (Version 9.3)*. Flow Science, Inc., Santa Fe, N. M.

Kouchakzadeh, S., & Townsend, R. (1997). Maximum scour depth at bridge abutments terminating in the floodplain zone. *Canadian Journal of Civil Engineering, 24*(6), 996–1006. https://doi.org/10.1139/cjce-24-6-996

Mahjoob, A., & Kilanehei, F. (2020). Effects of the skew angle and road embankment length on the hydraulic performance of bridges on compound channels. *Journal of the South African Institution of Civil Engineering, 62*(4). https://doi.org/10.17159/2309-8775/2020/v62n4a5

Mays, L. W. (2010). *Water Resources Engineering*. 2nd ed., Wiley, USA.

Molinas, A., Kheireldin, K., & Wu, B. (1998). Shear Stress around Vertical Wall Abutments. *Journal of Hydraulic Engineering, 124*(8), 822–830. https://doi.org/10.1061/(asce)0733-9429(1998)124:8(822)

Morales, R., & Ettema, R. (2013). Insights from Depth-Averaged Numerical Simulation of Flow at Bridge Abutments in Compound Channels. *Journal of Hydraulic Engineering, 139*(5), 470–481. https://doi.org/10.1061/(asce)hy.1943-7900.0000693

Seckin, G. (2007). The effect of skewness on bridge backwater prediction. *Canadian Journal of Civil Engineering, 34*(10), 1371–1374. https://doi.org/10.1139/l07-053

Shahhosseini, M., & Yu, G. (2019). Experimental Study on the Effects of Pier Shape and Skew Angle on Pier Scour. *Journal of Physics: Conference Series, 1300*, 012031. https://doi.org/10.1088/1742-6596/1300/1/012031

Shiono, K., & Knight, D. W. (1988, July). Two-dimensional analytical solution for a compound channel. In *Proceedings of 3rd international symposium on refined flow modelling and turbulence measurements* (pp. 503–510). Universal Academy Press.

Smith, H. D., & Foster, D. L. (2005). Modeling of Flow Around a Cylinder Over a Scoured Bed. *Journal of Waterway, Port, Coastal, and Ocean Engineering, 131*(1), 14–24. https://doi.org/10.1061/(asce)0733-950x(2005)131:1(14)

Vui Chua, K., Fraga, B., Stoesser, T., Ho Hong, S., & Sturm, T. (2019). Effect of Bridge Abutment Length on Turbulence Structure and Flow through the Opening. *Journal of Hydraulic Engineering, 145*(6), 04019024. https://doi.org/10.1061/(asce)hy.1943-7900.0001591

Wardhana, K., & Hadipriono, F. C. (2003). Analysis of Recent Bridge Failures in the United States. *Journal of Performance of Constructed Facilities, 17*(3), 144–150. https://doi.org/10.1061/(asce)0887-3828(2003)17:3(144)

Yang, Y., Melville, B. W., Macky, G. H., & Shamseldin, A. Y. (2019). Local Scour at Complex Bridge Piers in Close Proximity under Clear-Water and Live-Bed Flow Regime. *Water, 11*(8), 1530. https://doi.org/10.3390/w11081530

Zevenbergen, L. W., Arneson, L. A., Hunt, J. H., Miller, A. C., Ayres Associates, United States. Federal Highway Administration. Office of Bridge Technology, National Highway Institute (U.S.), Ayres Associates, United States. Federal Highway Administration. Office of Bridge Technology, & National Highway Institute (U.S.). (2012). *Hydraulic Design of Safe Bridges*. U.S. Department of Transportation, Federal Highway Administration, National Highway Institute.